



Interseismic deformation associated with three-dimensional faults in the greater Los Angeles region, California

Scott T. Marshall,¹ Michele L. Cooke,² and Susan E. Owen³

Received 6 March 2009; revised 14 May 2009; accepted 2 September 2009; published 9 December 2009.

[1] Existing interseismic models are not well-suited to simulate deformation within the network of finite, intersecting, nonplanar faults observed in the greater Los Angeles region. Instead of applying fault slip rates to a model a priori, we allow three-dimensional fault surfaces to interact and accumulate mechanically viable slip distributions and then use the deep nonseismogenic portion of slip to calculate interseismic deformation. We apply this approach to the Los Angeles region and find that the geologic timescale model results match well geologic slip rate data and the interseismic timescale model results match well the heterogeneous GPS velocity pattern in the Los Angeles region. Model results suggest that localized geodetic convergence in the San Gabriel basin can be achieved with slip on multiple active fault surfaces in the Los Angeles region including relatively fast slip on the Sierra Madre fault and slow slip on the Puente Hills thrusts, in agreement with geologic data. The ability of the three-dimensional model to reproduce well both geologic slip rates and interseismic geodetic velocity patterns suggests that current day contraction rates in the greater Los Angeles region are compatible with long-term geologic deformation rates and disputes suggestions of significant temporal variations in fault slip rates inferred from existing investigations.

Citation: Marshall, S. T., M. L. Cooke, and S. E. Owen (2009), Interseismic deformation associated with three-dimensional faults in the greater Los Angeles region, California, *J. Geophys. Res.*, *114*, B12403, doi:10.1029/2009JB006439.

1. Introduction

[2] Plate boundary scale models of interseismic deformation have matched much of the available geodetic data and have provided key insights into fault slip rates, strain partitioning, and seismic hazards in southern California [e.g., *Becker et al.*, 2005; *Bird and Kong*, 1994; *McCaffrey*, 2005; *Meade and Hager*, 2005; *Saucier and Humphreys*, 1993; *Savage and Burford*, 1973; *Shen et al.*, 1996], but these models often simplify the details of deformation within the complexly faulted Los Angeles region. The Los Angeles metropolitan region hosts a complex network of northwest trending strike-slip and reverse faults of the Peninsular ranges as well as west trending reverse faults of the transverse ranges [*Wright*, 1991]. Oversimplification of the fault geometry may account for many discrepancies between the slip rates inferred by these large models and slip rates determined from geologic observations. For example, block models of *Meade and Hager* [2005] predict reverse slip rates of 4.2 ± 0.9 mm/yr for the Puente Hills thrust, while indirect geologic evidence suggests 0.44–1.7 mm/yr of reverse slip [i.e., *Shaw et al.*, 2002]. Smaller

scope, two-dimensional models of planar faults also match aspects of the geodetic signal in the Los Angeles region [i.e., *Argus et al.*, 2005], but the results of such models suggest 9 ± 2 mm/yr of slip on the Puente Hills thrust, a rate over four times larger than that inferred from geologic data.

[3] Simplifications in interseismic deformation models often arise from difficulties in investigating discontinuous fault systems. For example, block model representations require continuous and connected fault networks [e.g., *Becker et al.*, 2005; *McCaffrey*, 2005; *Meade and Hager*, 2005], and two-dimensional models [e.g., *Argus et al.*, 2005; *Donnellan et al.*, 1993; *Hager et al.*, 1999] imply that faults are infinite in length. Such models do not accurately represent the discontinuous and imbricate faults revealed by seismic reflection [e.g., *Shaw et al.*, 2002] and geologic data [e.g., *Wright*, 1991] throughout the greater Los Angeles region (Figure 1) and may lead to inaccurate seismic hazard assessment.

[4] While conventional interseismic models utilizing semi-infinite dislocations [e.g., *Savage and Burford*, 1970; *Savage and Burford*, 1973; *Savage*, 1983] are useful for quantifying deformation associated with very long and isolated faults, this approach becomes problematic for multiple nonparallel fault surfaces where extending the faults to infinite depth requires fault intersections [e.g., *Shen et al.*, 1996]. Kinematic inverse methods [e.g., *Custódio et al.*, 2005; *Fialko*, 2004a; *Hearn and Bürgmann*, 2005; *Kaverina et al.*, 2002; *Maerten et al.*, 2005; *Price and Bürgman*, 2002; *Simons et al.*, 2002] that determine fault slip rates at depth from geodetic velocities encounter

¹Department of Geology, Appalachian State University, Boone, North Carolina, USA.

²Geosciences Department, University of Massachusetts Amherst, Amherst, Massachusetts, USA.

³Jet Propulsion Laboratory, Pasadena, California, USA.

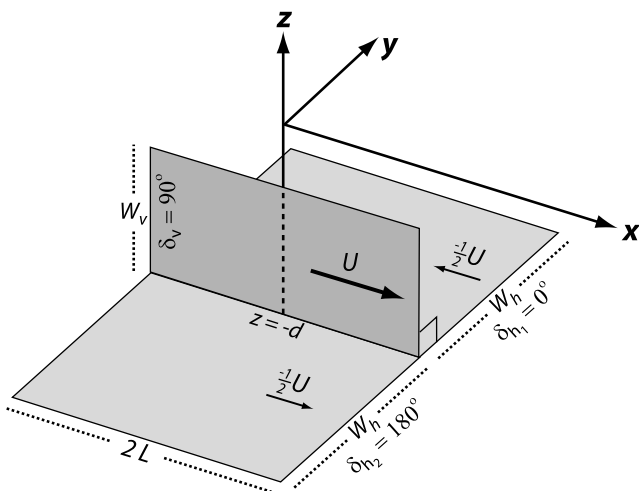


Figure 2. Coordinate system and dislocation parameters (following Okada [1985]) used to derive analytical solutions. We take the limit of Okada [1985] solutions as dislocation dimensions (L and W) approach infinity and compare to the interseismic solution of Savage and Burford [1973].

afterslip and relaxation) in southern California are limited to only several years after a major earthquake [e.g., Donnellan *et al.*, 2002; Fialko, 2004b]. Within the Los Angeles basin the last major earthquake was in 1994 (Northridge), therefore, postseismic transients are likely negligible. Furthermore, several recent deformation models of southern California [e.g., Becker *et al.*, 2005; Fay and Humphreys, 2005; Meade and Hager, 2005] suggest that the viscosity of the asthenosphere beneath southern California appears to be rather high ($>10^{19}$ Pa s), effectively reducing the importance of time-dependent effects throughout typical interseismic periods of southern California faults. Consequently, for most of the interseismic cycle, a linear elastic rheology can capture the first-order deformation mechanics of the seismogenic crust in southern California.

[7] In conventional elastic interseismic models, a vertical fault, extending to infinite depth, is embedded in an elastic half-space [e.g., Savage and Burford, 1970, 1973]. Below the locking depth, D , the fault undergoes steady state creep with a slip rate equal to the secular plate velocity, U . Along a semi-infinite vertical strike-slip fault, steady state, sub-seismogenic fault creep during the interseismic period results in fault-parallel displacements, u_x , at the surface of the Earth that are continuous across the fault and are described by

$$u_x = \left(\frac{-U}{\pi} \right) \arctan\left(\frac{y}{D}\right) \quad (1)$$

where y is the distance from the fault trace [Savage and Burford, 1973].

2.2. An Equivalent Dislocation Model

[8] In order to derive a model of interseismic deformation that is better suited for intersecting and nonparallel faults, we use the solutions of Okada [1985] for finite rectangular

dislocations to set up an interseismic model equivalent to the conventional solution.

[9] For a single vertical dislocation, as horizontal fault length (L) and vertical width (W) approach infinity, the fault-parallel motion approaches the analytical solution of Savage and Burford [1973]. Alternatively, if the vertical dislocation has infinite length, but finite vertical height and, at its base, joins with two horizontal dislocations with opposing displacements (see Figure 2), the surface displacements also approach the conventional solution as the horizontal dislocations approach infinite height and length (Figure 3). For this configuration of three dislocations, the surface displacements are independent of the depth to the horizontal dislocations and exactly replicate the surface displacements of the conventional model (see Appendix A for the detailed solution). This solution demonstrates that semi-infinite dislocation width of vertical strike-slip faults can be simulated by slip on horizontal dislocations at any depth. Additional parallel strike slip faults can be accommodated with additional horizontal dislocations between the faults. To incorporate nonparallel faults the horizontal dislocation between the faults must have nonuniform slip and for complex fault networks, the mechanically consistent slip distribution cannot be known a priori. The two-step numerical methodology that we use bypasses this problem by first, solving for the slip along all fault surfaces, including a freely slipping basal crack, and then applying the deep slip from that solution to the interseismic model.

2.3. Advantage of the Basal Horizontal Dislocation

[10] The analytical solution presented in the previous section effectively simulates deformation due to slip on semi-infinite vertical strike-slip faults; however, many of faults in the Los Angeles region are moderately dipping

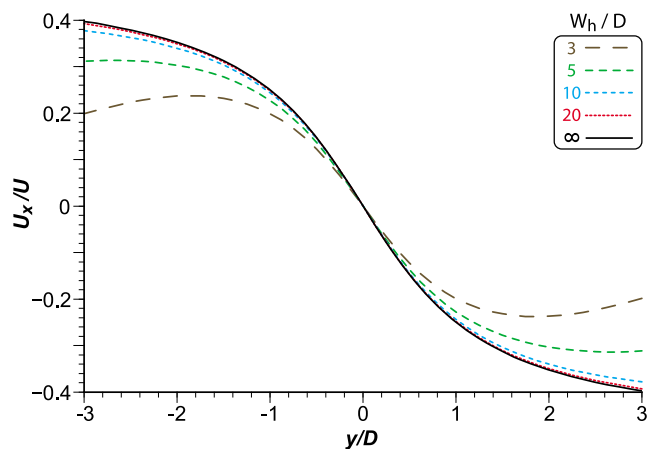


Figure 3. Fault-parallel displacements at the free surface from the dislocation geometry shown in Figure 2 are plotted for various horizontal dislocation widths (i.e., W_h in Figure 2). Horizontal dislocation widths are normalized by locking depth, D , and fault-parallel displacements, U_x , are normalized by fault slip rate, U . From this plot, we determine that joining a vertical fault with horizontal dislocations (see Figure 2) that extend to greater than 20 locking depths away should adequately reproduce the effects of an infinitely tall strike-slip fault so long as velocities are sampled within a few locking depths of the vertical fault.

reverse faults. If allowed to open and interpenetrate (i.e., a thin plate model), the horizontal detachment can be used to simulate crustal-scale reverse faulting (e.g., subduction); however, in contrast to regions of crustal-scale reverse faulting, the active reverse faults within southern California are not imaged into the lower crust. The Los Angeles Regional Seismic Experiment seismic data reveals that reverse faults in the Los Angeles region are truncated by a subhorizontal midcrustal décollement [Fuis *et al.*, 2001, 2003]. Using elastic dislocation models, Shen *et al.* [1996] determined that geodetic data is best fit when southern California strike-slip faults are extended to infinite depth and the reverse faults in the Los Angeles region do not maintain their dip and are horizontal at depth. Consequently, the basal horizontal crack in our models provides two benefits. First, the horizontal crack mechanically unpins the lower tip lines of strike-slip faults, simulating infinite height (see Appendix A for detailed solution). Second, the deep horizontal crack simulates the truncated reverse fault structure observed in available seismic imagery [e.g., Fuis *et al.*, 2001, 2003] and allows reverse faults to slip horizontally at depth as suggested by Shen *et al.* [1996]. While the depth to the horizontal basal crack has no effect on strike-slip rates, dip slip rates increase with increasing depth to the horizontal crack. Thus, a shallower basal crack would reduce reverse slip rates. This formulation mimics the crustal structure of the Los Angeles region and provides an efficient way to simulate lower crustal deformation within a region containing many nonparallel active faults. We note that this particular geometric configuration may not apply to all regions of convergent active faulting.

[11] In all models presented here, we place the basal crack at 27.5 km depth, the approximate depth of the Moho in the region [Fuis *et al.*, 2001; Magistrale *et al.*, 2000]. The compositional contrast between the crust and mantle may facilitate development of a décollement. Although the depth of the horizontal crack has no effect on strike-slip fault slip rates nor distributions in the region (see Appendix A), we adopt a depth greater than 20 km for the crack because moderately dipping reverse faults have been observed to slip below 20 km depth during the 1994 Northridge earthquake [e.g., Carena and Suppe, 2002]. Based on the analysis of Shen *et al.* [1996] and results from existing models using a similar deep horizontal crack [Cooke and Marshall, 2006; Dair and Cooke, 2009; Marshall *et al.*, 2008; Meigs *et al.*, 2008], we expect the model predicted surface deformation to be relatively insensitive to our choice of 27.5 km depth for the horizontal crack.

3. Three-Dimensional Fault Network of the Greater Los Angeles Region

[12] The Los Angeles metropolitan region hosts a complex system of active faults (Figure 1). Northwest trending strike-slip and reverse faults of the Peninsular ranges abut west trending reverse faults of the transverse ranges [Wright, 1991] resulting in a network of obliquely intersecting active faults with complex three-dimensional surfaces [e.g., Plesch *et al.*, 2007]. Rather than simplify the complex strike-slip and reverse fault geometries in the Los Angeles region, we utilize the complex geologically constrained

fault surfaces of the Southern California Earthquake Center Community Fault Model (CFM) [Plesch *et al.*, 2007]. In models presented here, we utilize the CFM version 2.5, with several modifications described in detail in a previous work [i.e., Meigs *et al.*, 2008].

4. BEM Implementation of Interseismic Deformation

[13] In order to determine the distribution of slip along numerous interacting and intersecting three-dimensional faults in response to regional tectonic boundary conditions, we develop a boundary element method (BEM) implementation of interseismic deformation. The BEM is advantageous for complex fault geometries because only fault surfaces need to be discretized. To simulate deformation in the Los Angeles region, we utilize the angular dislocation program, Poly3D [Thomas, 1993], based on the Boundary Element Method [e.g., Comninou and Dunders, 1975]. In all models presented here, 33 Los Angeles region fault surfaces are discretized into triangular elements (5 km average diameter), which most efficiently reproduce complex three-dimensional surfaces [e.g., Maerten *et al.*, 2005; Meade, 2007]. Because the fault mesh is based upon the CFM, which utilizes spatially variable data density, some well-constrained fault surfaces have elements with diameters less than 1 km (see the interactive PDF file at <http://www.apstate.edu/~marshallst/pubs/LA3D.pdf>). All modeled fault elements are shear stress free and are not permitted to open or interpenetrate.

[14] We create interseismic models in a two-step process. First, we create a geologic time scale model simulating 5000 years of deformation where the entire fault surface slips. Then, in a second interseismic time scale model, we prescribe this distribution of slip along the faults with zero slip above the locking depth.

[15] In the first step, we simulate the accumulation of geologic deformation in the Los Angeles region. Instead of imposing slip rates or distributions [e.g., Argus *et al.*, 2005; Donnellan *et al.*, 1993; Shen *et al.*, 1996] or inverting for slip rates [e.g., Becker *et al.*, 2005; McCaffrey, 2005; Meade and Hager, 2005], we drive deformation from below [e.g., Dair and Cooke, 2009; Fay and Humphreys, 2005; Jolivet *et al.*, 2008] by applying displacements along the periphery of the basal dislocation at depth that reproduce geodetic strain rates in the modeled region. Once the tectonic boundary conditions are calibrated (i.e., the modeled region contracts at strain rates similar to the geodetic strain), we insert the CFM-based Meigs *et al.* [2008] fault geometry and allow faults to freely interact and accumulate mechanically viable slip distributions at all crustal levels in response to the imposed regional contraction. Because slip along many southern California faults is spatially variable [e.g., Dair and Cooke, 2009; Marshall *et al.*, 2008], this approach avoids producing mechanically unviable uniform slip rates along the finite faults in the Los Angeles region.

[16] In the second step of our methodology, we simulate interseismic deformation by removing slip within the locked seismogenic crust on modeled faults and apply the slip from the geologic model below a specified locking depth to an interseismic model. This two-step process resembles the back slip approach of Savage [1983], except that instead of

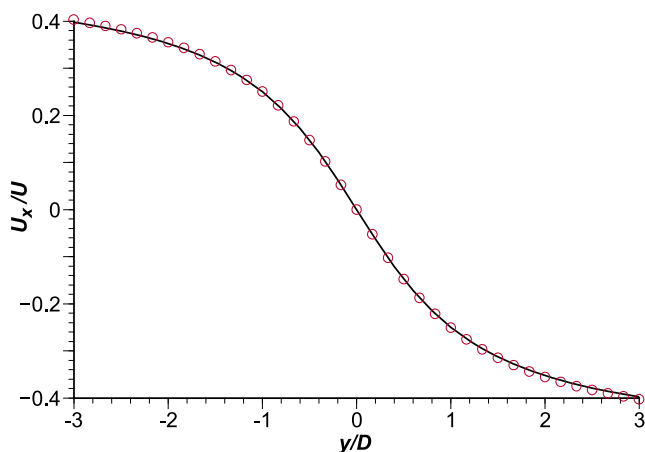


Figure 4. Analytical solution from equation (1) (line) and BEM model approximation (circles) of fault-parallel surface displacements at distance from an interseismic vertical strike-slip fault. As in Figure 3, fault-parallel motion, U_x , is normalized by fault slip rate, U , and distance from the vertical fault, y , is normalized by locking depth, D . The BEM model results are for a vertical fault that joins a 30 km deep horizontal dislocation. Because the modeled fault surfaces are discretized into a finite number of elements, small discrepancies between the analytical solution and numerical model reflect discretization errors.

subtracting a model with seismogenic slip from the geologic model, we simply set the seismogenic slip to zero and utilize the remaining portion of the geologic fault slip to directly solve for the interseismic deformation field. Interseismic velocities calculated at the free surface of the half-space can be directly compared to the corrected GPS velocities in the Los Angeles region.

[17] To demonstrate that the BEM implementation successfully reproduces the conventional interseismic model, we create a model with a single, very long strike-slip fault that merges into a large horizontal detachment at 30 km depth. To determine the geologic time scale slip rates and distribution, we apply fault-parallel displacements at the periphery of the horizontal crack at depth and allow the vertical fault to accumulate strike-slip motion at all depths [e.g., *Dair and Cooke, 2009*]. We then create an interseismic model by applying the slip from the geologic model to all modeled elements below a prescribed locking depth. We compare these numerical fault-parallel surface displacements to the conventional analytical solution of equation (1) (Figure 4). The BEM model matches well the conventional interseismic solution with small errors arising due to the finite discretization of the fault surfaces.

5. Geodetic Data and Tectonic Boundary Conditions

[18] In this study, we utilize the final corrected geodetic velocities reported by *Argus et al. [2005]* by selecting a subset of 49 permanent GPS sites and one trilateration site (BadPow) that lie within our region of interest (Figure 1). Because the *Argus et al. [2005]* geodetic velocities have the effects of the San Andreas and San Jacinto faults removed

from the geodetic signal, the San Andreas and San Jacinto faults are also omitted from our models.

[19] Surface deformation rates measured at geodetic stations in populated regions of southern California are complicated by anthropogenic and seasonal effects [e.g., *Bawden et al., 2001*]. In the greater Los Angeles region, *Argus et al. [2005]* isolated the local tectonic signal from the regional geodetic data by removing effects of the nearby San Andreas and San Jacinto faults as well as significant seasonal variations and anthropogenic motions that arise from subsurface fluid withdrawal and injection. Due to uncertainty in these corrections (dominantly due to the uncertainty in anthropogenic motions), the Los Angeles regional GPS velocities have typical 95% confidence limits of 1.5–3.5 mm/yr [*Argus et al., 2005*].

[20] We determine regional tectonic boundary conditions for the model from motions of permanent GPS stations at the edges of the Los Angeles region that have the effects of the San Andreas and San Jacinto faults, fluid pumping, and seasonal effects removed [i.e., *Argus et al., 2005*]. Stations at the Palos Verdes peninsula (PVEP, VTIS, PVHS, PVR5) are moving ~ 6 mm/yr northward relative to the San Gabriel mountain stations ~ 80 km away, yielding an average regional shortening rate of ~ 72 nstrain/yr (nanostain per year) oriented at $N9^\circ E$. This interseismic strain rate neglects some motion on the locked portions of the Palos Verdes fault that would be observed if we had GPS stations offshore. Assuming a geologically reasonable 15 km locking depth and the maximum geologically estimated slip rate of 3.8 mm/yr, we estimate that the missing contractional strain could only be $<5\%$ larger than our regional estimate. Because the model utilized here is linear elastic, the model may underestimate fault slip rates by up to 5%; however, a 72 nstrain gradient fits most of the Los Angeles region GPS data well, therefore we choose the regionally consistent 72 nstrain strain rate to drive motion on faults in the region.

[21] To the geologic timescale models we apply displacement at depth along the periphery of the basal crack until the modeled region contracts at 72 nstrain/yr at $N9^\circ E$ orientation. This GPS-derived contraction rate and direction is similar to the tectonic boundary conditions that have shown good overall match to fault slip sense [*Griffith and Cooke, 2005*], fault slip rates [*Cooke and Marshall, 2006*], and patterns of uplift [*Meigs et al., 2008*] in the region.

6. Geologic Timescale Model: Comparison to Geologic Slip Rates

[22] To determine whether current day geodetic strain rates are compatible with geologic fault slip rates, we compare results from a geologic timescale model to available geologic estimates of fault slip rates. Small differences in reverse slip rates between the model results presented here and the results of *Cooke and Marshall [2006]* reflect improved application of boundary conditions. Artificial constraints on vertical strain in models of *Cooke and Marshall [2006]* restricted reverse slip. Most of the model-predicted strike and dip slip rates of models fall within the available paleoseismic ranges (Figure 5). Discrepancies between the model slip rates and the ranges of paleoseismic data occur along the Cucamonga, Northridge, Palos Verdes, and Raymond faults (Figure 5). The Cucamonga fault lies at

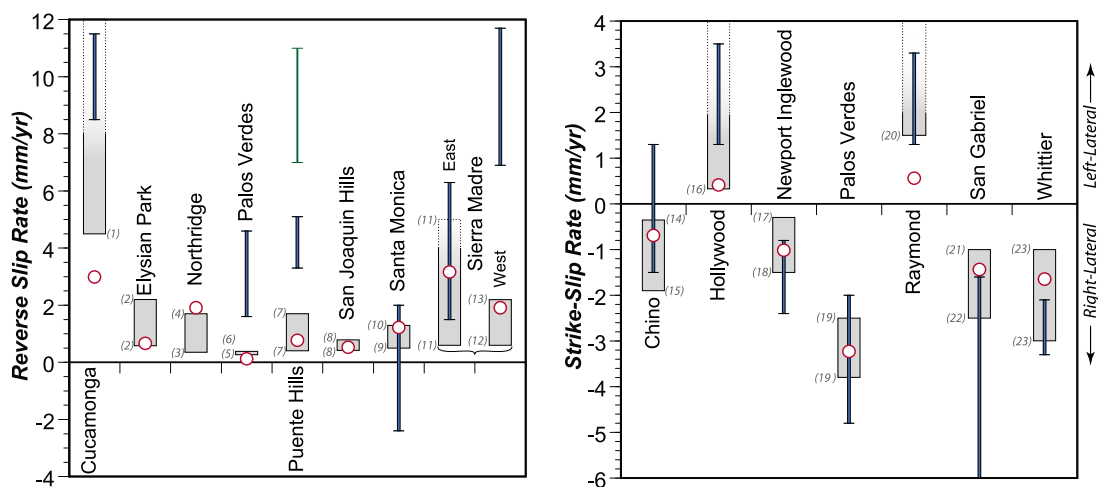


Figure 5. Model-predicted average slip rates (red circles) and geologic slip rate estimates (gray rectangular ranges). Gradient shading on geologic ranges indicate that the upper limit is poorly constrained. To calculate the average slip rate of modeled fault surface containing many elements of varying size, we integrate the slip over each element's area and calculate a weighted average slip rate for each surface. The Puente Hills reverse slip rate estimate of *Argus et al.* [2005] is shown with a green line, and slip rate estimates from the *Meade and Hager* [2005] block model are shown with thick blue lines. References for the upper and lower geologic slip rate ranges are shown by gray italic numbers and are as follows: (1) *Morton and Matti* [1987], (2) *Oskin et al.* [2000], (3) *Dolan et al.* [1997], (4) *Huftile and Yeats* [1996], (5) *Bryant* [1987], (6) *McNeilan et al.* [1996], (7) *Shaw et al.* [2002], (8) *Grant et al.* [1999], (9) *Dolan and Pratt* [1997] and *Dolan et al.* [2000], (10) *Tsutsumi et al.* [2001], (11) *Tucker and Dolan* [2001], (12) *Rubin et al.* [1998], (13) *Crook et al.* [1987], (14) *Walls and Gath* [2001], (15) *Yeats* [2002], (16) *Dolan et al.* [1997], (17) *Freeman et al.* [1992] and *Grant et al.* [1997], (18) *Lindvall and Rockwell* [1995], (19) *Stephenson et al.* [1995], (20) *Marin et al.* [2000], (21) *Kahle* [1986], (22) *Yeats et al.* [1994], and (23) *Gath et al.* [1992].

the eastern edge of the model adjacent to the San Andreas fault. Consequently, the slip rate discrepancy along the Cucamonga fault reflects that the fault lies at the edge of the model where interaction with faults to the east is neglected. Similarly, the Northridge thrust lies at the northwestern edge of our model where nearby active faults (e.g., Anacapa-Dume, Del Valle, Holser, Northridge Hills, and Santa Susana faults) not modeled here, would accommodate significant strain and reduce slip on the Northridge thrust.

[23] Discrepancies between geologic reverse slip rate estimates and average model calculated slip rate on the Palos Verdes fault reflect spatial variations in dip slip due to the nonplanar fault trace [*Cooke and Marshall*, 2006], suggesting that the geologic estimates of uplift along this fault were made in nonrepresentative locations. The model-predicted slip rates match well the geologic slip rates determined from uplift at the location of these estimates. Disagreement between geological and average model strike-slip rate along the Raymond fault may reflect incorrect fault geometry including differences in connectivity between the Raymond and Verdugo–Eagle Rock fault.

[24] The three-dimensional model fit to geologic slip rate data represents an improvement over existing block models [*Meade and Hager*, 2005] as well as existing two-dimensional models [*Argus et al.*, 2005] of the region. While the three-dimensional model presented here and the *Meade and Hager* [2005] block model fit geologic strike-slip rates nearly equally well, our three-dimensional model shows better agreement with geologic reverse slip data (see Figure 5). The block model approach appears to commonly

overestimate reverse slip rates compared to geologic estimates. Likewise, two-dimensional models of the Los Angeles region [i.e., *Argus et al.*, 2005], greatly overestimate geologic slip rates on the Puente Hills thrust compared to geologic data.

[25] The overall close match of model-calculated average fault slip rates to paleoseismic data suggests that the geologic model performs well and captures the primary features of geologic deformation in the Los Angeles region. Next, we utilize this geologic timescale model to create an interseismic model of the Los Angeles region and compare results to geodetic data.

7. Interseismic Model Results

7.1. Locking Depth Sensitivity

[26] To simulate interseismic deformation, we apply the distribution of slip calculated in the geologic timescale model on fault elements below a prescribed locking depth with all fault elements locked above this depth. Because earthquake data suggests a relatively consistent locking depth throughout the region [e.g., *Richards-Dinger and Shearer*, 2000], we only test uniform locking depths. We test a range of locking depths from 5 to 27 km to determine the locking depth that best fits the geodetic data. Because the geodetic velocities have varying error magnitudes, we weight the model-GPS residuals by the geodetic velocity errors reported by *Argus et al.* [2005] and compute the weighted residual root-mean-square error (WRMS) for a range of locking depths (Figure 6). The WRMS values

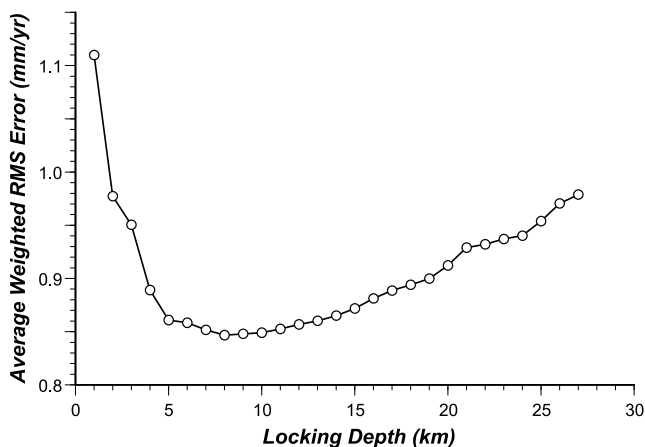


Figure 6. Average weighted residual RMS errors for interseismic models of the Los Angeles region utilizing various locking depths. Although an 8 km locking depth minimizes the weighted RMS error, locking depths of 5–13 km do not provide significantly worse overall match to GPS velocities.

suggest a best fitting locking depth of 8 km; however, the fit to GPS data is relatively insensitive to locking depths between 5 and 15 km, suggesting that our models do not constrain well the locking depth in the Los Angeles region. The ~ 0.85 mm/yr RMS of the best fitting model suggests that the interseismic model, on average, matches geodetic velocities at the sub mm/yr level, well within the typical 1–3 mm/yr reported 95% confidence levels reported by *Argus et al.* [2005].

7.2. Interseismic Surface Velocities

[27] The three-dimensional interseismic model produces a similar surface velocity pattern to the GPS data (Figure 7). Variations from a $N9^{\circ}E$ orientation indicate distortional strain due to strike-slip faulting (e.g., near the Newport-Inglewood and Palos Verdes faults) and variations from a linear velocity gradient indicate localized convergence (e.g., eastern San Gabriel basin). While the best fitting model matches all GPS velocities in the region within the 95% confidence limits, discrepancies greater than 2.5 mm/yr between the model surface movement and GPS velocities occur at stations BKMS, FXHS, LPHS, and SACY, which highlight the four main areas of mismatch: the northern Los Angeles basin, the Whittier Hills, the San Gabriel basin, and the San Joaquin Hills (Figure 8).

[28] Relatively large residuals may arise from model simplifications and errors in fault geometry. At locations of high residuals, nearby GPS stations show significantly different velocity vector azimuth; this local distortion may indicate local strike-slip faulting. However, the fastest strike-slip faults in the model, Palos Verdes and Newport-Inglewood, do not locally distort the surface velocity pattern as much as observed in the four main areas of model and observation mismatch (Figure 7). If the observed distortion were due to missing slip on faults, this strike slip would have to both greatly exceed 4 mm/yr and only occur on small portions of faults limited to the regions of distortion.

Such fast and localized slip is mechanically unviable and thus unlikely in the region. Alternatively, relatively large horizontal residuals may reflect lingering nontectonic signals in the corrected geodetic data of *Argus et al.* [2005] because gradients in uplift rates produce horizontal motions away from the direction of the uplift gradient (the converse is true for subsidence). Furthermore, the same vertical motions may produce horizontal deformation that may vary by a factor of two depending on the geometry of the deforming body [*Fialko et al.*, 2001]. Such a correction scheme is nontrivial in the Los Angeles region where anthropogenic groundwater removal results in localized subsidence and temporally variable subsurface fluid removal and injection in active oil fields produces subsidence and uplift, respectively. For example, *Argus et al.* [2005] state that stations BKMS, FXHS, LPHS, and RHCL may have been undercorrected for anthropogenic and seasonal effects, possibly by a factor of ~ 2 . We discuss four regions of relatively large residuals in detail, to better elucidate whether the relatively large residuals reflect inaccurate GPS velocities, an inadequacy of the deformation model, or a combination of these two effects.

[29] The model produces relatively large residuals at stations near the Whittier Hills (BKMS, WHC1, DYHS, and RHCL). Station WHC1 in the Whittier hills shows more easterly azimuth than the nearby stations to the west, suggesting missing interseismic right-lateral strain accumulation along a NW-SE trending fault; however, to match this gradient, the slip on such a fault would have to far exceed the geologic estimates of 1–3 mm/yr on the Whittier fault. Alternatively, because stations BKMS, WHC1, and DYHS are located on unconsolidated alluvial deposits and are thus potentially susceptible to motions caused by changes in groundwater or oil reservoirs (RHCL is on sedimentary bedrock and is less susceptible), residuals may reflect improperly characterized nontectonic motion in the GPS velocities. All of the sites near the Whittier Hills exhibit azimuths that have been significantly altered by the anthropogenic correction technique of *Argus et al.* [2005]. The residuals at sites DYHS and BKMS are directed toward the Santa Fe Springs oil field (location 1 on Figure 8) where InSAR data show localized uplift rates of up to 10 mm/yr, indicative of significant subsurface fluid injection [*Argus et al.*, 2005]. The residual vectors at DYHS and BKMS from our model are strikingly similar to the inferred anthropogenic vectors of *Argus et al.* [2005]. If we remove the anthropogenic corrections of *Argus et al.* [2005] at these sites, our residuals are reduced to less than 1 mm/yr at both sites, suggesting possible overcorrection of anthropogenic motion. In contrast, the nearby station WHC1 may have been undercorrected for anthropogenic motion. Like the nearby stations, the azimuth of the correction for WHC1, due to pumping at the Whittier Hills oil fields, parallels the residual of our model results; however removing the correction would increase rather than decrease the residuals of our model.

[30] The model produces a relatively large surface velocity residual at station FXHS in the northern Los Angeles basin (location 2 on Figure 8). The GPS velocity at station FXHS has an azimuth significantly different from neighboring stations (Figure 7) that would require very fast

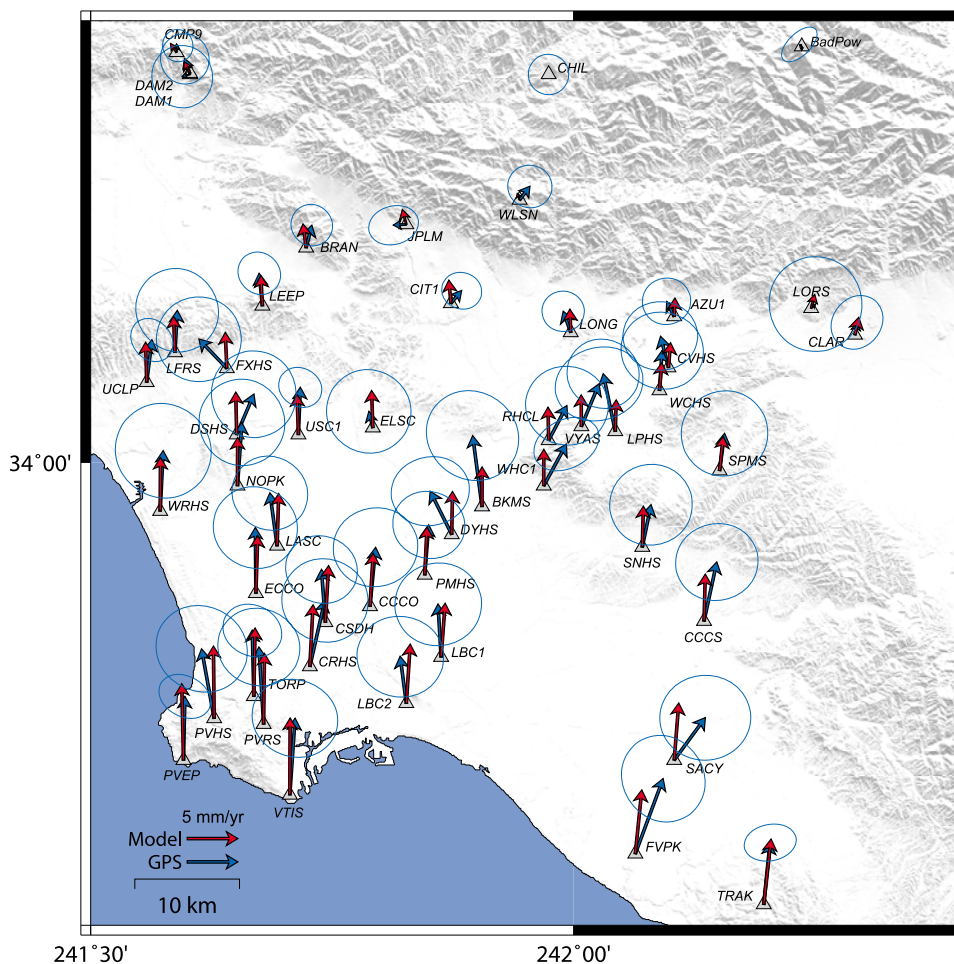


Figure 7. Permanent GPS (blue arrows) and model-calculated (red arrows) interseismic velocities in the greater Los Angeles region. Errors in corrected velocities are given by *Argus et al.* [2005] with the 95% confidence ellipses shown here. Model results are shown for a locking depth of 8 km which minimizes the WRMS error (Figure 6) and matches all GPS velocities within the 95% confidence limits. The largest discrepancies arise near the Whittier Hills (sites BKMS, WHC1, RHCL, VYAS, and LPHS), the San Joaquin Hills fault (near site FVPK and SACY), and at a site near the San Vicente and Hollywood faults in the northern Los Angeles basin (sites FXHS).

strike-slip rates along a hypothetical fault if this gradient was due to missing interseismic slip. Furthermore, the change in GPS velocity azimuth between station FXHS and nearby LFRS is consistent with right-lateral slip accumulating across the Hollywood and Santa Monica faults in contrast to the known kinematics of these left-lateral faults [Dolan and Pratt, 1997; Dolan et al., 1997]. Alternatively, the velocity of site FXHS (located on unconsolidated alluvium) may reflect mischaracterized anthropogenic motion associated with localized ~ 10 mm/yr of subsidence in the nearby Salt Lake oil fields. The inferred horizontal anthropogenic motion from 1992 to 1999 and 1998–2000 at site FXHS differs by $\sim 90^\circ$ of azimuth [cf. *Argus et al.*, 2005, Figure 5–6], suggesting a temporally complex pumping history in nearby oil fields. Furthermore, the net inferred anthropogenic correction of FXHS points in approximately the opposite direction as our residual at this site (consistent with overcorrection of anthropogenic effects), suggesting that the relatively large residual at

FXHS likely represents mischaracterization of anthropogenic motion.

[31] Near the San Joaquin Hills, the discrepancy between GPS and model results may also arise from mischaracterized anthropogenic motions by *Argus et al.* [2005]. Stations SACY and FVPK are located on unconsolidated sediments above the Santa Ana aquifer, which produces large nontectonic subsidence of up to ~ 10 mm/yr associated with groundwater removal [Argus et al., 2005]. The model residuals at sites SACY and FVPK both point away from the location of maximum subsidence in the Santa Ana aquifer (location 3 on Figure 8) consistent with overcorrection of these sites for nontectonic motions.

[32] The residuals of stations VYAS, LPHS, WCHS, CYHS, and AZU1 (all located on unconsolidated sediments) generally point away from the center of the San Gabriel Basin where InSAR data from 1998 to 2000 [i.e., *Argus et al.*, 2005] show substantial subsidence associated with groundwater removal (location 4 on Figure 8). Like the

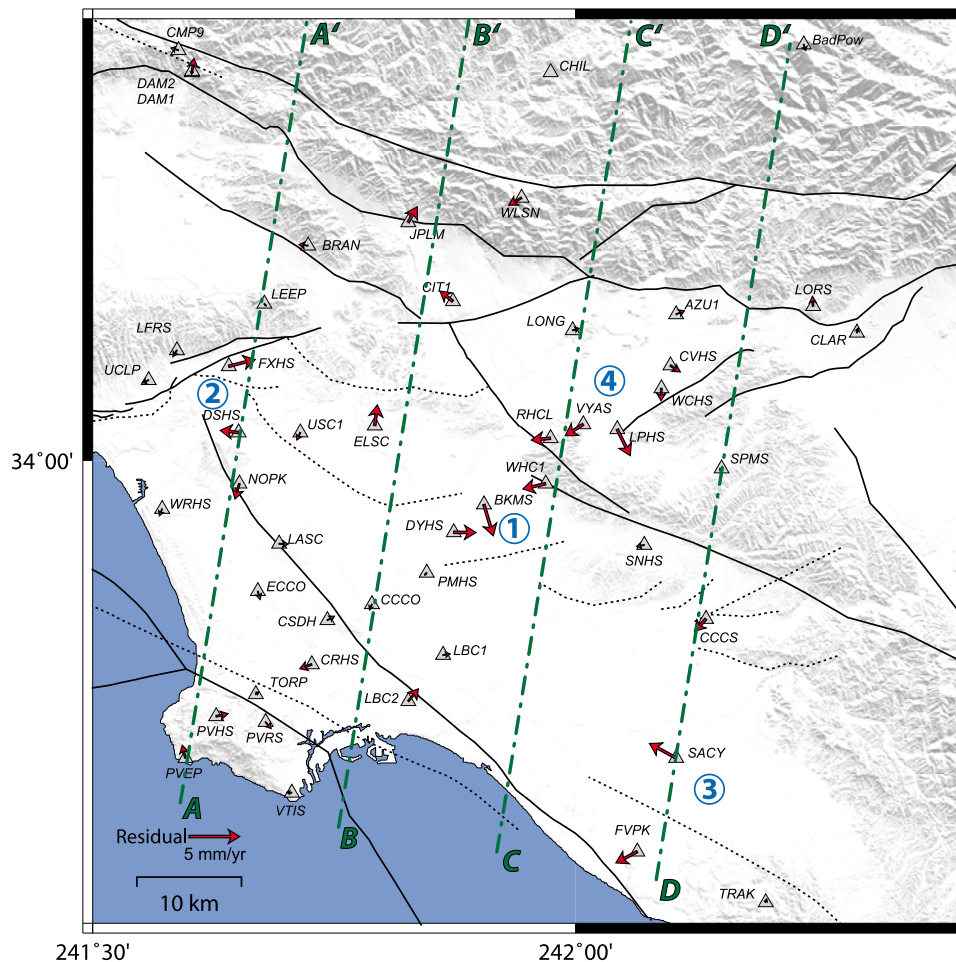


Figure 8. Model-GPS residuals for model with 8 km locking depth. The vector scale is the same as Figure 7. The four areas of greatest residuals discussed in the text are labeled and correspond to local maxima of anthropogenic subsidence or uplift: (1) location of maximum uplift due to fluid injection in the Santa Fe Springs oil fields near the Whittier Hills, (2) location of maximum subsidence due to fluid extraction in the Salt Lake oil fields near the northern Los Angeles basin, (3) location of maximum subsidence from groundwater removal in the Santa Ana aquifer near the San Joaquin Hills, and (4) location of maximum subsidence due to groundwater removal in the San Gabriel basin aquifer. In all four regions, insufficient correction of seasonal and anthropogenic effects may account for the high residuals. Sites in these regions were also characterized as contaminated by anthropogenic motions by *Bawden et al.* [2001]. The locations of four N9°E oriented, 80 km long, and 15 km spaced transects through the region are shown with green dot-dashed lines.

Santa Ana aquifer, this pattern of residuals is consistent with overcorrection of horizontal motion in GPS velocities due to nontectonic subsidence.

8. Discussion

8.1. Model and GPS Transects

[33] Some features of the geodetic surface velocities, such as zones of localized contraction, can be most clearly delineated using two-dimensional transects of the region. While projecting the GPS stations to linear transects removes the rich patterns shown on Figures 7 and 8, we present transects to show how localized contraction that has previously been attributed to reverse slip on the Puente Hills thrust [i.e., *Argus et al.*, 2005] could instead be attributed to reverse slip along a variety of structures including the relatively fast slipping Sierra Madre fault.

[34] Four 80 km long transects oriented at N9°E across the greater Los Angeles area show the correlation of GPS station velocity and transects through the three-dimensional interseismic model (Figure 9). The transects are not perpendicular to most of the regional faults, but follow the direction of the regional contraction because obliquely loaded faults will slip with oblique slip. Within all four transects, the three-dimensional interseismic model velocities match the geodetic pattern of convergence across the greater Los Angeles region within the 95% confidence limits with the single exception of a minor discrepancy with site JPLM in transect A.

[35] Regional shortening in the Los Angeles region is accommodated by both off fault deformation (e.g., folding [*Davis and Namson*, 1994; *Meigs et al.*, 2008; *Oskin et al.*, 2000]) as well as slip on a network of discontinuous faults

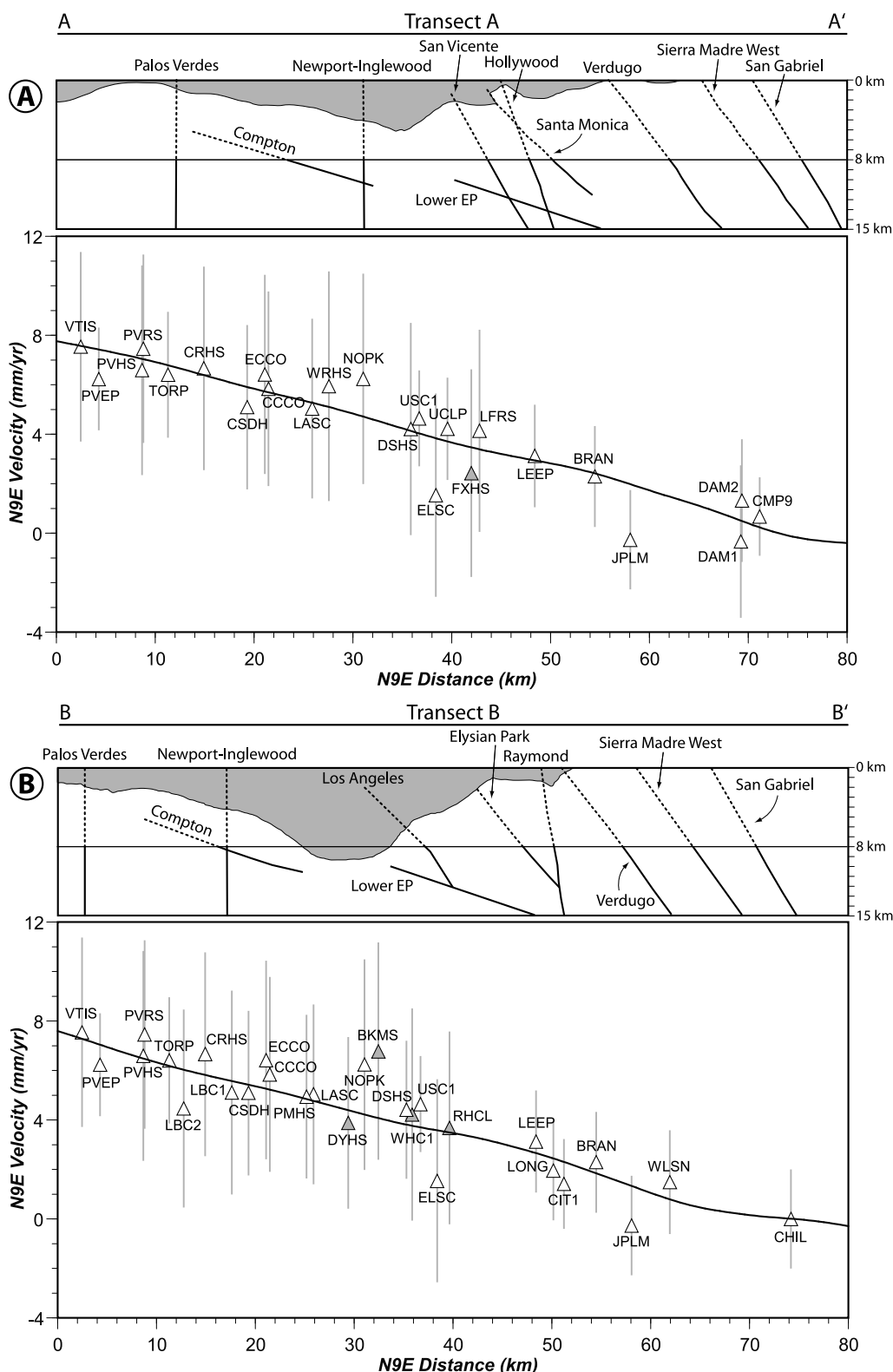


Figure 9. N9°E transects (A and B) through the Los Angeles region showing model and GPS velocities. Locations of transects are shown on Figure 8. A cross-sectional slice through the three-dimensional model along each transect is shown above each plot with faults shown with black lines (dashed where locked). Sedimentary basins are shaded gray. The N9°E component of GPS velocities and station location are projected onto transects (triangles). Vertical gray lines indicate the N9°E component of the 95% confidence limits. GPS stations discussed in the text that potentially have mischaracterized anthropogenic motion are shown with gray triangles. Model results are shown with black curves. Localized convergence is strongest in the eastern transects (C and D) in both the model and GPS data.

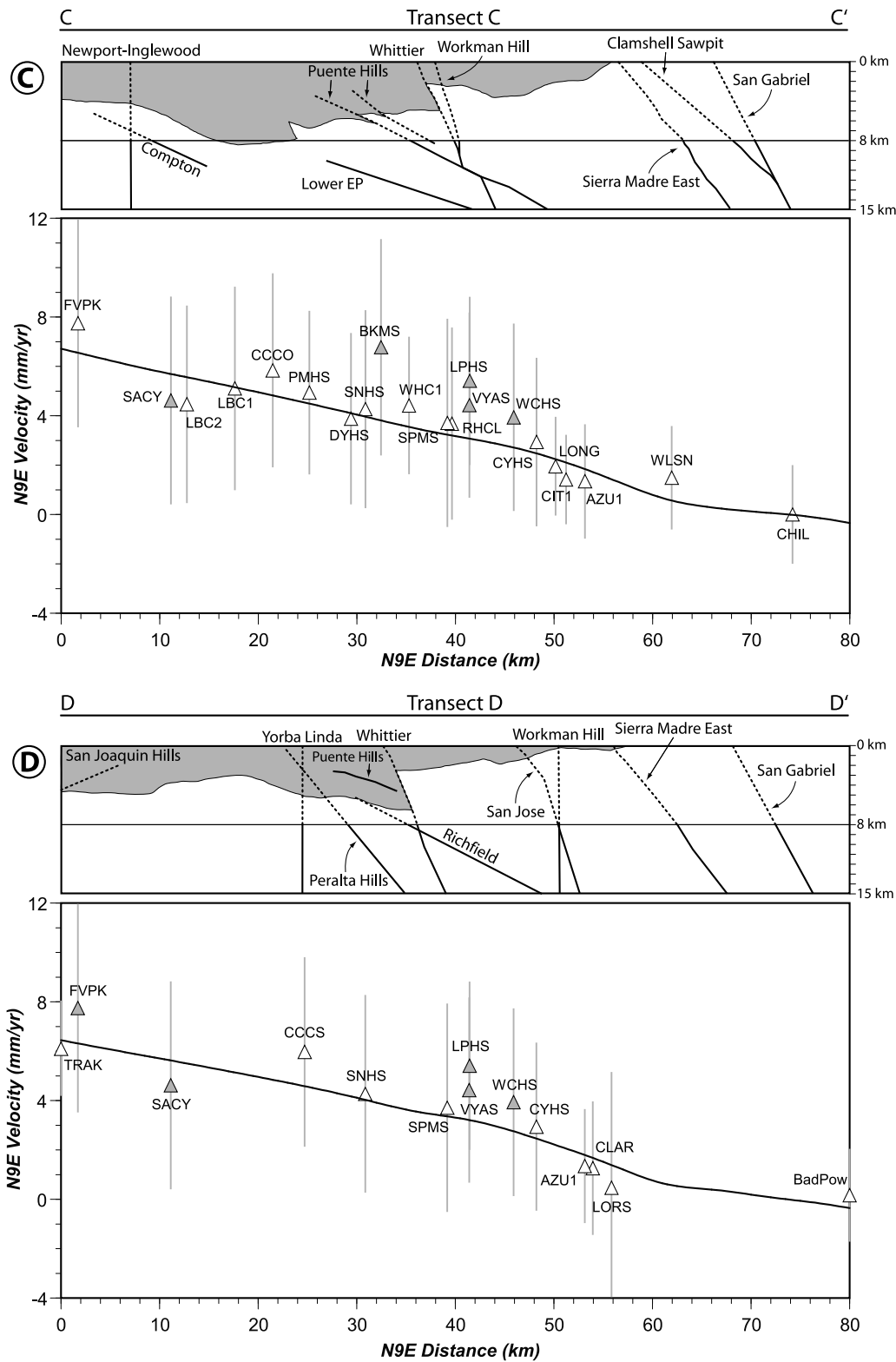


Figure 9. (continued)

whereby each individual fault accommodates a small portion of the regional deformation. Therefore, relatively slow slip across numerous faults in the Los Angeles region results in nearly linear velocity gradients with the only clear deviation from a linear gradient occurring around 50–60 km on Figure 9.

[36] In general, convergence is more distributed in the western transects (A and B) than in the eastern transects (C and D), where N9°E convergence is localized within the northern San Gabriel basin near station AZU1. Slip along numerous imbricate thrust faults (San Gabriel, Sierra Madre, Verdugo, Santa Monica, Hollywood, and the Puente

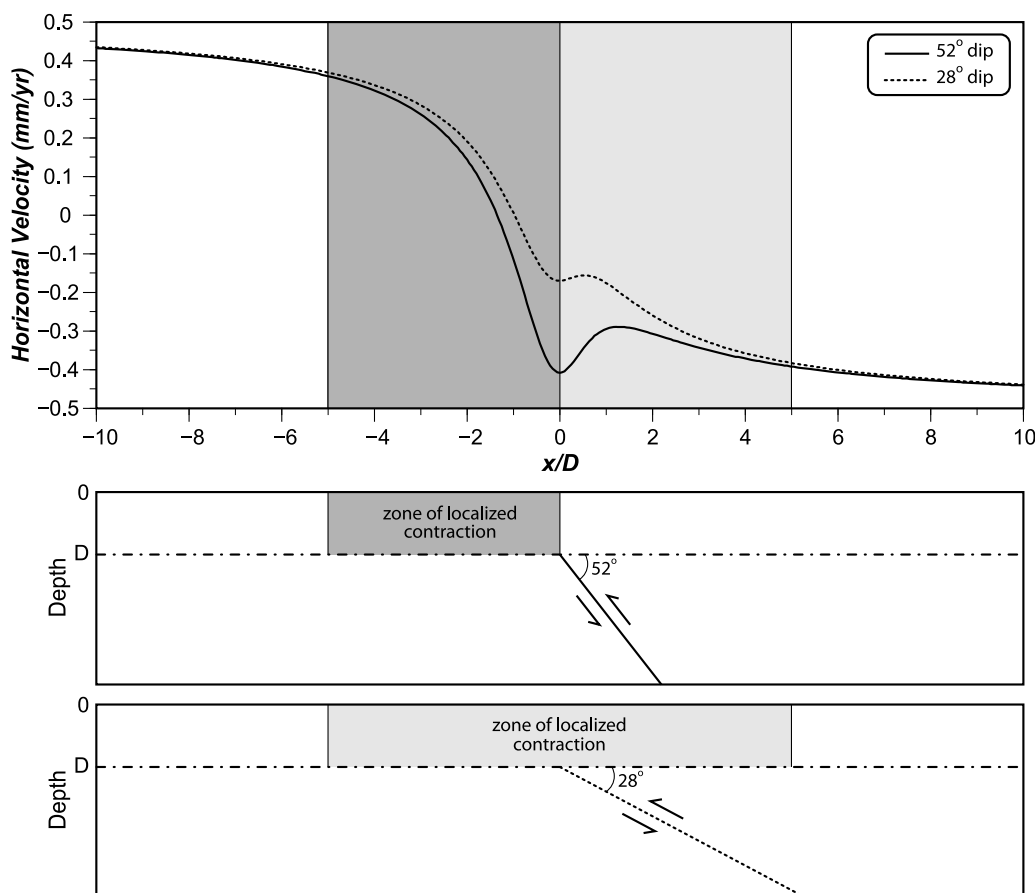


Figure 10. Surface velocity normal to a reverse fault trace due to slip on a semi-infinite reverse fault following *Freund and Barnett* [1976] and *Savage and Simpson* [1997]. We plot the surface velocities for two fault dips: 52° (average dip of the Sierra Madre fault, solid line) and 28° (the average dip of the Puente Hills thrust, dashed line). Both curves are shown for a regional horizontal contraction of 1 mm/yr. For shallow dipping faults such as the Puente Hills thrust, a zone of localized contraction is centered on the upper tip of the slipping fault and extends from $\sim -5D$ to $5D$. On reverse faults with more moderate dip such as the Sierra Madre fault, the edge of the zone of localized contraction is located above the slipping fault tip (i.e., $0D$) and extends to $\sim -5D$. Although both fault dips plotted above produce small localized zones of extension from $0D$ to $\sim D$, such a small amount of extension is not likely to be resolved given current error limits on geodetic data and the relatively slow fault slip rates in the region.

Hills thrust faults) within transect A and B may account for the more distributed N 9° E surface convergence relative to transect C and D, where convergence is primarily associated with fewer faults (the Sierra Madre, Puente Hills, and Lower Elysian Park faults).

[37] A zone of localized convergence observed in the GPS velocities lies to the south of the upper tip of the creeping portion Sierra Madre fault (see Figures 9c and 9d). Though the 95% confidence limits of most of the GPS data do not tightly constrain this localized convergence, this convergence has been used to infer 9 ± 2 mm/yr slip on the Puente Hills Thrust Fault [i.e., *Argus et al.*, 2005]. Reverse faults of shallow dip ($< \sim 40^\circ$) such as the Puente Hills thrust (average dip $\sim 28^\circ$) produce relatively similar amounts of contraction in both the hanging wall and footwall above the fault tip. In contrast, slip along moderately dipping ($> 45^\circ$) reverse faults produces greater contraction rates in the footwall block than in the hanging wall block above the fault tip [e.g., *Freund and Barnett*, 1976]. Consequently, a zone of high contraction can be attributed

to either slip along a low dipping fault with tip directly below the center of the zone or slip along a moderately dipping reverse faults with the fault tip to the side of the contracting zone (Figure 10). Although *Argus et al.* [2005] fit the GPS data well with slip along the Puente Hills that are 8 times faster than geologically inferred rates, the zone of convergence could also be fit with a moderately dipping fault with a tip below the northern edge of the contracting zone (e.g., the Sierra Madre Fault). The geologic evidence of relatively fast slip on the Sierra Madre fault and slow slip on the Puente Hills fault agrees with our three-dimensional model results and adequately reproduces the geodetic velocities.

[38] The zone of fast convergence in transects C and D of Figure 9 contains sites that may have significant remnant nontectonic motions. If one ignores the velocities at these potentially inaccurate sites (the gray triangles on Figure 9), the convergence across this zone may be reduced by nearly 50%. Given the large range in the 95% confidence limits to the GPS data, the data cannot rule out either the interpre-

tation of fast slip along the Puente Hills fault or the interpretation of fault slip along the Sierra Madre fault. Because our model can reproduce the general features of the GPS velocity field as well as remain compatible with numerous independent geologic data sets (slip rate estimates, fault geometries), we advocate that our model represents an improvement over the *Argus et al.* [2005] and *Meade and Hager* [2005] models.

8.2. Deformation in Sedimentary Basins and Locking Depth Discrepancies

[39] A seismogenic locking depth of 8 km for the greater Los Angeles region disagrees with observations of seismicity at depths up to 20 km [*Richards-Dinger and Shearer*, 2000]. Based on analysis of locking depth sensitivity (Figure 6), we cannot rule out locking depths greater than the best fitting 8 km. Locking depths shallower than the base of seismicity have been determined from several elastic dislocation models of southwestern California [e.g., *Argus et al.*, 2005; *Donnellan et al.*, 1993]. *Hager et al.* [1999] suggest that models incorporating compliant sedimentary basin material are necessary to fit localized convergence rates in the Ventura basin with reasonable locking depth. Because the only significant gradients in the GPS velocities are found in the San Gabriel basin, where the sedimentary basin fill is relatively thin (see Figure 9), incorporating heterogeneous rock properties to our model may not improve fit to geodetic velocities in the region. If the seismogenic locking depth in the model were greater, the localized convergence in transects C and D due to the Sierra Madre fault would become more diffuse and the position would shift to the north, producing greater mismatch to the GPS data. This northward shift could be offset by the strain localizing effect of compliant (less stiff) sedimentary basin fill, which is greatest in the southern portion of the San Gabriel basin. However, if the model were to incorporate variations in rock stiffness, convergence rates in transects A and B (where the Los Angeles trough is of greater depth) may also be altered, possibly producing a zone of localized convergence in the model that is not clearly observed in the geodetic data. Therefore, adding spatially varying rock stiffness to the model may not improve fit to GPS data.

[40] Incorporation of heterogeneous rock properties does not universally improve model fit to geodetic data. For example, *Fay and Humphreys* [2005] determine that including lateral and vertical variations in rock stiffness reduce model fit to geodetic data in the Salton Trough. In other models of the same region, *Fialko* [2006] shows that differences in rock stiffness across the mapped locations of the southern San Andreas and San Jacinto faults can improve fit to geodetic data in the region, but only if the inferred rigidity contrasts exceed (by a factor of 2–2.5) estimated rock stiffness contrast inferred from seismic tomography data in the region [e.g., *Hauksson*, 2000]. Alternatively, *Fialko* [2006] suggests that an east dipping San Andreas fault could also reproduce the asymmetric velocity profile with geologically viable variations in rock stiffness. The east dip of the San Andreas fault has since been documented by relocated seismicity [*Lin et al.*, 2007], suggesting that precise knowledge of fault geometry is essential to accurately model surface deformation. Where fault geometry is well known and relatively simple, such as

along the Carrizo segment of the San Andreas fault, models incorporating variations in rock properties and crustal thickness are required to match asymmetric surface deformation rates [*Schmalzle et al.*, 2006]. While fault geometry and heterogeneous properties may both contribute to variations in geodetic velocities, we must first accurately establish the three-dimensional configuration of the fault network before we can assess heterogeneous properties. Whether the presence of complex three-dimensional sedimentary basins in the Los Angeles Basin significantly affects active deformation remains unclear. A detailed parametric study of various theoretical and well-constrained three-dimensional basins is necessary to provide insight into ongoing deformation in the complex three-dimensional sedimentary basins of the Los Angeles region.

8.3. Implications for Short- and Long-Term Deformation

[41] Using two-dimensional dislocation models, *Argus et al.* [2005] fit the location and rate of localized convergence in the San Gabriel basin with 9 mm/yr of reverse slip along the Puente Hills thrust fault. This slip rate exceeds the geologic slip rate estimated from analysis of suprafault growth strata (0.4–1.7 mm/yr [*Shaw et al.*, 2002]). Likewise many reverse slip rates determined from the block model of *Meade and Hager* [2005] also overestimate reverse slip rates. The simplified and overconnected nature of faulting in the block model as well as the permission of interpenetration of fault surfaces to simulate dip slip may have led to the overprediction. Our three-dimensional models demonstrate that the regional GPS velocities can be matched within the 95% confidence limits with geologically reasonable slip rates on nearly all faults in the region including ~ 0.8 mm/yr average reverse slip on the Puente Hills Thrust (Figure 5). These results suggest that the current day interseismic shortening rates in the Los Angeles region are compatible with long-term geologic estimates. Temporal variations in fault loading rates have been proposed to explain slip rate discrepancies between geodetic analyses and geologic observations [e.g., *Dolan et al.*, 2007; *Huffile and Yeats*, 1995, 1996; *Oskin et al.*, 2008; *Yeats*, 1978]. Such complications are not necessary in the Los Angeles basin where discrepancies between long-term slip rates and slip rates inferred from short-term geodesy may a product of oversimplification of fault geometry within past models.

9. Conclusions

[42] We formulate an analytical model of interseismic deformation associated with strike-slip faulting that reproduces the surface displacements of the conventional interseismic solution without extending faults to infinite depth. Based on this solution, we implement a two-step numerical forward modeling approach that can be used to quantify geologic and interseismic deformation rates due to slip on complex three-dimensional fault surfaces of arbitrary shape and size in the Los Angeles region. We demonstrate the utility of this technique by simulating geologic and interseismic deformation along the complex network of fault surfaces in the greater Los Angeles region. Model results match well both geologic slip rate estimates and interseis-

mic GPS velocities in the region, suggesting that the models capture the first-order features of geologic and interseismic deformation in the region. Most regions where the interseismic model produces relatively high residuals occur where GPS stations likely have mischaracterized anthropogenic and seasonal motions, suggesting that corrected GPS velocities may better elucidate the current day tectonic deformation pattern in the Los Angeles region. The uncertainties in the GPS data cannot distinguish between a model with fast slip on the Puente Hills thrust or fast slip on the Sierra Madre fault. We advocate that the three-dimensional model proposed herein, while more complex than the models of *Argus et al.* [2005], represents an improvement because the model is compatible with numerous types of geologic data (fault geometries and slip rate data) as well as GPS data.

[43] The close correlation of three-dimensional interseismic model predictions of surface velocities with geodetic data and the match of geologic model predictions of fault slip rates with geologic data suggest little discrepancy between geodetic and geologic deformation rates in the metropolitan Los Angeles region. In contrast to results from two-dimensional models of the region that evoke geologically discrepant slip rates of 9 mm/yr [*Argus et al.*, 2005] or 4.2 mm/yr [*Meade and Hager*, 2005] on the Puente Hills fault, we find that localized convergence in the San Gabriel basin can be produced by a three-dimensional model with relatively fast slip on the Sierra Madre fault and relatively slow slip on the Puente Hills thrusts, in agreement with geologic slip rate estimates. Furthermore, although the models here employ homogeneous and isotropic material properties, the complex fault structure produces a heterogeneous pattern of deformation throughout the Los Angeles region, suggesting that two-dimensional analyses of the region may have limited suitability.

Appendix A: Analytical Solutions for an Equivalent Interseismic Model

[44] To demonstrate that the dislocation setup in Figure 2 reproduces the conventional interseismic displacement profile of a semi-infinite vertical fault [i.e., *Savage and Burford*, 1973], we use the analytical solutions of *Okada* [1985] for finite rectangular faults and find the limit of various solutions as the dislocations approach infinite dimensions. Our notation follows from *Okada* [1985]. For a single vertical fault of infinite length and width located along the x axis the fault-parallel surface displacements are described by equation (1).

[45] For a vertical fault of finite width that joins with two horizontal dislocations at depth, $-d$, each having equal and opposite senses of displacement (Figure 2), the net, fault-parallel surface displacement field can be found by finding the sum of the contributions from each of the three dislocations. The fault-parallel displacement at the free surface of a semi-infinite half-space arising in response to uniform strike slip over a vertical rectangular dislocation of finite width, W_1 , is given by

$$u_x = \frac{-U}{2\pi} \left[\frac{\xi y}{R_v(R_v + \eta)} + \arctan\left(\frac{\xi \eta}{y R_v}\right) + I \right] \parallel_v \quad (\text{A1})$$

where

$$\begin{cases} I = -\frac{\mu}{2(\lambda + \mu)} \frac{\xi y}{(R + \eta)^2} \\ R_v^2 = \xi^2 + \eta^2 + y^2 \end{cases} \quad (\text{A2})$$

and \parallel_v represents the substitution,

$$u_x(\xi, \eta) = u_x(x + L, d) - u_x(x + L, D) - u_x(x - L, d) + u_x(x - L, D) \quad (\text{A3})$$

where U is the slip on the fault, μ and λ are Lamé parameters, D is the locking depth, and W , L , and d are as shown in Figure 2. Substituting infinity for L (i.e., an infinitely long fault) and after algebraic simplification, we arrive at the solution for the fault-parallel displacement along the y axis due to the finite width vertical fault,

$$u_x = \frac{-U}{\pi} \left[\arctan\left(\frac{y}{D}\right) - \arctan\left(\frac{y}{d}\right) \right] \quad (\text{A4})$$

[46] This agrees with existing solutions for a fault of finite height [e.g., *Savage*, 1980, 1990]. This solution only differs from (1) in that an additional term, $-\arctan(y/d)$, is present to account for the finite height of the fault. Therefore, to simulate an infinitely tall fault (i.e., $W \rightarrow \infty$, $d \rightarrow \infty$) the two horizontal dislocations must counteract this additional term.

[47] For a $\delta = 0$ horizontal dislocation with a uniform strike-slip displacement of $-U/2$, the fault-parallel displacement at the free surface is given by

$$u_x = \frac{-U}{4\pi} \left[\frac{-\xi d}{R_h(R_h + \eta)} + \arctan\left(\frac{-\xi \eta}{d R_h}\right) \right] \parallel_{h1} \quad (\text{A5})$$

where \parallel_{h1} represents the substitution,

$$u_x(\xi, n) = u_x(x + L, y) - u_x(x + L, y - W) - u_x(x - L, y) + u_x(x - L, y - W) \quad (\text{A6})$$

where

$$R_h^2 = \xi^2 + \eta^2 + d^2 \quad (\text{A7})$$

and all other terms are the same as above. Upon substitution of infinity for L and W (simulating a semi-infinite horizontal dislocation), and after algebraic simplification, we arrive at the contribution to the fault-parallel displacement field at the free surface due to strike slip on the horizontal dislocation,

$$u_x = \frac{-U}{2\pi} \left[\arctan\left(\frac{-y}{d}\right) - \frac{\pi}{2} \right] \quad (\text{A8})$$

[48] For the other horizontal dislocation ($\delta = 180$), the equations for the fault-parallel displacement at the free surface are similar to (A5) and (A6) (equation (A10) does not change), except that changing the angle, δ , to 180, results in y and ξ becoming negative in sign. Note that the sign of the displacement need not change since changing

the dislocation angle, δ , from 0 to 180 effectively reverses the sense of strike slip on the dislocation. As before, after substitution of infinity for L and W , and after algebraic simplification, we arrive at the contribution to fault parallel motion from the second horizontal crack,

$$u_x = \frac{-U}{2\pi} \left[\arctan\left(\frac{-y}{d}\right) + \frac{\pi}{2} \right] \quad (\text{A9})$$

[49] Summing the contributions from both of the horizontal cracks (equations (A10) and (A11)), we arrive at the contribution from both basal horizontal cracks,

$$u_x = \left(\frac{-U}{2\pi} \right) \arctan\left(\frac{-y}{d}\right) \quad (\text{A10})$$

Summing the displacement contributions from each of the three dislocations in Figure 2 (equations (1), (A10), and (A11)), we arrive at

$$u_x = \left(\frac{-U}{\pi} \right) \arctan\left(\frac{-y}{D}\right) \quad (\text{A11})$$

Thus, the contribution from both horizontal cracks exactly cancels out the second arctan term in (A4) resulting in the total fault-parallel motion due to the three cracks equaling the conventional solution for a vertical semi-infinite strike-slip fault. The sum effect of the horizontal dislocation setup shown in Figure 2 is independent of depth to the horizontal dislocations. For this reason, the depth to the horizontal dislocations is unimportant for strike-slip faults. We also note that because the strain due to a dislocation is only due to the dislocation edge, the conventional arctangent profile of equation (1) can be reproduced with any pair of arbitrarily dipping basal dislocations so long as they have the same slip and share an edge along the lower tip of the vertical fault.

[50] **Acknowledgments.** This work was partially supported by U.S. Geological Survey (USGS), Department of the Interior, under USGS award 05HQGR0064. This research was also partially supported by the Southern California Earthquake Center. SCEC is funded by NSF Cooperative Agreement EAR-0106924 and USGS Cooperative Agreement 02HQAG0008. The SCEC contribution for this paper is 1168. This work benefited greatly from discussions with Eric Hetland on an early version of this work and with Don Argus concerning geodetic data corrections. We thank Chris Walls for detailed site geology of several key GPS stations. Constructive reviews by Jean Chéry and three anonymous reviewers greatly improved this work. Poly3D was made available by IGEOS. Manipulation of fault surfaces was facilitated by use of 3DMove by Midland Valley Ltd. Figures 1, 7, and 8 were generated with the assistance of Generic Mapping Tools [Wessel and Smith, 1998].

References

Argus, D. F., M. B. Heflin, G. Peltzer, F. Crampé, and F. H. Webb (2005), Interseismic strain accumulation and anthropogenic motion in metropolitan Los Angeles, *J. Geophys. Res.*, *110*, B04401, doi:10.1029/2003JB002934.

Bawden, G. W., et al. (2001), Tectonic contraction across Los Angeles after removal of groundwater pumping effects, *Nature*, *412*, 812–815, doi:10.1038/35090558.

Becker, T. W., et al. (2005), Constraints on fault slip rates of the southern California plate boundary from GSA velocity and stress inversions, *Geophys. J. Int.*, *160*, 634–650, doi:10.1111/j.1365-246X.2004.02528.x.

Bird, P., and X. Kong (1994), Computer simulations of California tectonics confirm very low strength of major faults, *Geol. Soc. Am. Bull.*, *106*, 159–174, doi:10.1130/0016-7606(1994)106<0159:CSOCTC>2.3.CO;2.

Bryant, M. E. (1987), Emergent marine terraces and Quaternary tectonics, Palos Verdes Peninsula, California, in *SEPM Guidebook*, edited, pp. 63–78.

Bryant, M. E. (1987), Emergent marine terraces and Quaternary tectonics Palos Verdes Peninsula, California, in *Geology of the Palos Verdes Peninsula and San Pedro Bay, SEPM Guideb.*, vol. 55, edited by P. J. Fischer, pp. 63–78, Pac. Sect., Soc. of Econ. Paleontol. and Mineral., Los Angeles, Calif.

Carena, S., and J. Suppe (2002), Three-dimensional imaging of active structures using earthquake aftershocks: The Northridge thrust, California, *J. Struct. Geol.*, *24*, 887–904, doi:10.1016/S0191-8141(01)00110-9.

Comninou, M. A., and J. Dunders (1975), The angular dislocation in a half-space, *J. Elast.*, *5*, 203–216, doi:10.1007/BF00126985.

Cooke, M. L., and S. T. Marshall (2006), Fault slip rates from three-dimensional models of the Los Angeles metropolitan area, California, *Geophys. Res. Lett.*, *33*, L21313, doi:10.1029/2006GL027850.

Crook, R., Jr., et al. (1987), Quaternary geology and seismic hazard of the Sierra Madre and associated faults, western San Gabriel Mountains, in *Recent Reverse Faulting in the Transverse Ranges, California*, edited by D. M. Morton and R. F. Yerkes, *U.S. Geol. Surv. Prof. Pap.*, *1339*, 27–63.

Custódio, S., P. Liu, and R. J. Archuleta (2005), The 2004 M_w 6.0 Parkfield, California, earthquake: Inversion of near-source ground motion using multiple data sets, *Geophys. Res. Lett.*, *32*, L23312, doi:10.1029/2005GL024417.

Dair, L., and M. L. Cooke (2009), San Andreas fault geometry through the San Geronio Pass, California, *Geology*, *37*(2), 119–122, doi:10.1130/G25101A.1.

Davis, T. L., and J. S. Namson (1994), A balanced cross section analysis of the 1994 Northridge earthquake and thrust fault seismic hazards in Southern California, *Seismol. Res. Lett.*, *65*, 3–4.

Dixon, T. H., E. Norabuena, and L. Hotaling (2003), Paleoseismology and Global Positioning System: Earthquake-cycle effects and geodetic versus geologic fault slip rates in the eastern California shear zone, *Geology*, *31*(1), 55–58, doi:10.1130/0091-7613(2003)031<0055:PAGPSE>2.0.CO;2.

Dolan, J. F., and T. L. Pratt (1997), High-resolution seismic reflection profiling of the Santa Monica fault zone, west Los Angeles, California, *Geophys. Res. Lett.*, *24*(16), 2051–2054, doi:10.1029/97GL01940.

Dolan, J. F., K. Sieh, T. K. Rockwell, P. Gupta, and G. Miller (1997), Active tectonics, paleoseismology, and seismic hazards of the Hollywood fault, Los Angeles basin, California, *Geol. Soc. Am. Bull.*, *109*(12), 1595–1616, doi:10.1130/0016-7606(1997)109<1595:ATPASH>2.3.CO;2.

Dolan, J. F., K. Sieh, and T. K. Rockwell (2000), Late Quaternary activity and seismic potential of the Santa Monica fault system, Los Angeles, California, *Geol. Soc. Am. Bull.*, *112*, 1559–1581, doi:10.1130/0016-7606(2000)112<1559:LQAASP>2.0.CO;2.

Dolan, J., D. D. Bowman, and C. G. Sammis (2007), Long-range and long-term fault interactions in southern California, *Geology*, *35*(9), 855–858, doi:10.1130/G23789A.1.

Donnellan, A., B. H. Hager, and R. W. King (1993), Discrepancy between geological and geodetic deformation rates in the Ventura Basin, *Nature*, *366*(6453), 333–336, doi:10.1038/366333a0.

Donnellan, A., J. W. Parker, and G. Peltzer (2002), Combined GPS and InSAR models of postseismic deformation from the Northridge earthquake, *Pure Appl. Geophys.*, *159*, 2261–2270, doi:10.1007/s00024-002-8734-7.

Fay, N. P., and E. D. Humphreys (2005), Fault slip rates, effects of elastic heterogeneity on geodetic data, and the strength of the lower crust in the Salton Trough region, southern California, *J. Geophys. Res.*, *110*, B09401, doi:10.1029/2004JB003548.

Fialko, Y. (2004a), Probing the mechanical properties of seismically active crust with space geodesy: Study of the coseismic deformation due to the 1992 M_w 7.3 Landers (southern California) earthquake, *J. Geophys. Res.*, *109*, B03307, doi:10.1029/2003JB002756.

Fialko, Y. (2004b), Evidence of fluid-filled upper crust from observations of postseismic deformation due to the 1992 M_w 7.3 Landers earthquake, *J. Geophys. Res.*, *109*, B08401, doi:10.1029/2004JB002985.

Fialko, Y. (2006), Interseismic strain accumulation and the earthquake potential on the southern San Andreas fault system, *Nature*, *441*, 968–971, doi:10.1038/nature04797.

Fialko, Y., Y. Khazan, and M. Simons (2001), Deformation due to a pressurized horizontal circular crack in an elastic half-space, with applications to volcano geodesy, *Geophys. J. Int.*, *146*, 181–190, doi:10.1046/j.1365-246X.2001.00452.x.

Freeman, S. T., E. G. Heath, P. D. Gupta, and J. T. Wagoner (1992), Seismic hazard assessment, Newport-Inglewood fault zone, in *Engineering Geology Practice in Southern California, Spec. Publ.*, vol. 4, edited by W. B. Popkin and R. J. Proctor, pp. 211–230, Assoc. of Eng. Geol., Belmont, Calif.

Freund, L. B., and D. M. Barnett (1976), A two-dimensional analysis of surface deformation due to dip-slip faulting, *Bull. Seismol. Soc. Am.*, *66*(3), 667–675.

- Fuis, G. S., T. Ryberg, N. J. Godfrey, D. A. Okaya, and J. M. Murphy (2001), Crustal structure and tectonics from the Los Angeles basin to the Mojave Desert, southern California, *Geology*, 29(1), 15–18, doi:10.1130/0091-7613(2001)029<0015:CSATFT>2.0.CO;2.
- Fuis, G. S., et al. (2003), Fault systems of the 1971 San Fernando and 1994 Northridge earthquakes, southern California: Relocated aftershocks and seismic images from LARSE II, *Geology*, 31(2), 171–174, doi:10.1130/0091-7613(2003)031<0171:FSOTSF>2.0.CO;2.
- Gath, E. M., T. Gonzalez, and T. K. Rockwell (1992), Slip rate of the Whittier Fault based on 3-D trenching at Brea, southern California, *Geol. Soc. Am. Abstr. Programs*, 24, 26.
- Grant, L. B., J. T. Waggoner, T. K. Rockwell, and C. von Stein (1997), Paleoseismicity of the north branch of the Newport-Inglewood fault zone in Huntington Beach, California, from cone penetrometer test data, *Bull. Seismol. Soc. Am.*, 87, 277–293.
- Grant, L. B., K. J. Mueller, E. M. Gath, H. Cheng, R. L. Edwards, R. Munro, and G. L. Kennedy (1999), Late Quaternary uplift and earthquake potential of the San Joaquin Hills, southern Los Angeles basin, California, *Geology*, 27(11), 1031–1034, doi:10.1130/0091-7613(1999)027<1031:LQUAEP>2.3.CO;2.
- Griffith, W. A., and M. L. Cooke (2005), How sensitive are fault slip rates in the Los Angeles Basin to tectonic boundary conditions?, *Bull. Seismol. Soc. Am.*, 95(4), 1263–1275, doi:10.1785/0120040079.
- Hager, B. H., G. A. Lyzenga, A. Donnellan, and D. Dong (1999), Reconciling rapid strain accumulation with deep seismogenic fault planes in the Ventura Basin, California, *J. Geophys. Res.*, 104(B11), 25,207–25,219, doi:10.1029/1999JB900184.
- Hammond, W. C., and W. Thatcher (2007), Crustal deformation across the Sierra Nevada, northern Walker Lane, Basin and Range transition, western United States measured with GPS, 2000–2004, *J. Geophys. Res.*, 112, B05411, doi:10.1029/2006JB004625.
- Hauksson, E. (2000), Crustal structure and seismicity distribution adjacent to the Pacific and North American plate boundary in southern California, *J. Geophys. Res.*, 105, 13,875–13,903, doi:10.1029/2000JB900016.
- Hearn, E. H., and R. Bürgmann (2005), The effect of elastic layering on inversions of GPS data for coseismic slip and resulting stress changes: Strike-slip earthquakes, *Bull. Seismol. Soc. Am.*, 95(5), 1637–1653, doi:10.1785/0120040158.
- Hetland, E. A., and B. H. Hager (2003), Postseismic relaxation across the Central Nevada Seismic Belt, *J. Geophys. Res.*, 108(B8), 2394, doi:10.1029/2002JB002257.
- Hetland, E. A., and B. H. Hager (2006), Interseismic strain accumulation: Spin-up, cycle invariance, and irregular rupture sequences, *Geochem. Geophys. Geosyst.*, 7, Q05004, doi:10.1029/2005GC001087.
- Hufnagle, G. J., and R. S. Yeats (1995), Convergence rates across a displacement transfer zone in the western Transverse Ranges, Ventura Basin, California, *J. Geophys. Res.*, 100(B2), 2043–2067, doi:10.1029/94JB02473.
- Hufnagle, G. J., and R. S. Yeats (1996), Deformation rates across the Placerita (Northridge $M_w = 6.7$ aftershock zone) and Hopper Canyon segments of the western Transverse Ranges deformation belt, *Bull. Seismol. Soc. Am.*, 86(1), 3–18.
- Jolivet, R., R. Cattin, N. Chamot-Rooke, C. Lasserre, and G. Peltzer (2008), Thin-plate modeling of interseismic deformation and asymmetry across the Altyn Tagh fault zone, *Geophys. Res. Lett.*, 35, L02309, doi:10.1029/2007GL031511.
- Kahle, J. E. (1986), The San Gabriel fault near Castaic and Saugus, Los Angeles County, *Fault Eval. Rep. FER 178*, 8 pp., Calif. Div. of Mines and Geol., Sacramento.
- Kaverina, A., D. Dreger, and E. Price (2002), The combined inversion of seismic and geodetic data for the source of the 16 October $M_w 7.1$ Hector Mine, California, earthquake, *Bull. Seismol. Soc. Am.*, 92(4), 1266–1280, doi:10.1785/0120000907.
- King, G. C. P., R. S. Stein, and J. Lin (1994), Static stress changes and the triggering of earthquakes, *Bull. Seismol. Soc. Am.*, 84, 935–953.
- Lin, G., P. M. Shearer, and E. Hauksson (2007), Applying a three-dimensional velocity model, waveform cross correlation, and cluster analysis to locate southern California seismicity from 1981 to 2005, *J. Geophys. Res.*, 112, B12309, doi:10.1029/2007JB004986.
- Lindvall, S. C., and T. K. Rockwell (1995), Holocene activity of the Rose Canyon fault zone in San Diego, California, *J. Geophys. Res.*, 100, 24,121–24,132, doi:10.1029/95JB02627.
- Maerten, F., P. Resor, D. Pollard, and L. Maerten (2005), Inverting for slip on three-dimensional fault surfaces using angular dislocations, *Bull. Seismol. Soc. Am.*, 95, 1654–1665, doi:10.1785/0120030181.
- Magistrale, H., S. Day, R. W. Clayton, and R. Graves (2000), The SCEC southern California reference three-dimensional seismic velocity model version 2, *Bull. Seismol. Soc. Am.*, 90(6B), S65–S76, doi:10.1785/0120000510.
- Marin, M., et al. (2000), A latest Pleistocene-Holocene slip rate on the Raymond fault based on 3-D trenching, East Pasadena, California, *Eos Trans. AGU*, 81(48), Fall Meet. Suppl., F855.
- Marshall, S. T., M. L. Cooke, and S. E. Owen (2008), Effects of non-planar fault topology and mechanical interaction on fault slip distributions, *Bull. Seismol. Soc. Am.*, 98(3), 1113–1127, doi:10.1785/0120070159.
- McCaffrey, R. (2005), Block kinematics of the Pacific–North America plate boundary in the southwestern United States from inversion of GPS, seismological, and geologic data, *J. Geophys. Res.*, 110, B07401, doi:10.1029/2004JB003307.
- McNeilan, T. W., T. K. Rockwell, and G. S. Resnick (1996), Style and rate of Holocene slip, Palos Verdes fault, southern California, *J. Geophys. Res.*, 101(B4), 8317–8334, doi:10.1029/95JB02251.
- Meade, B. J. (2007), Algorithms for the calculation of exact displacements, strains, and stresses in a uniform elastic half space, *Comput. Geosci.*, 33, 1064–1075, doi:10.1016/j.cageo.2006.12.003.
- Meade, B. J., and B. H. Hager (2005), Block models of crustal motion in southern California constrained by GPS measurements, *J. Geophys. Res.*, 110, B03403, doi:10.1029/2004JB003209.
- Meigs, A. J., M. L. Cooke, and S. T. Marshall (2008), Using vertical rock uplift patterns to infer and validate the three-dimensional fault configuration in the Los Angeles basin, *Bull. Seismol. Soc. Am.*, 98(1), 106–123, doi:10.1785/0120060254.
- Morton, D. M., and J. C. Matti (1987), The Cucamonga fault zone: Geologic setting and Quaternary history, in *Recent Reverse Faulting in the Transverse Ranges, California*, edited by D. M. Morton and R. F. Yerkes, *U.S. Geol. Surv. Prof. Pap.*, 1339, 179–203.
- Okada, Y. (1985), Surface deformation due to shear and tensile faults in a half-space, *Bull. Seismol. Soc. Am.*, 75(4), 1135–1154.
- Oskin, M., K. Sieh, T. Rockwell, G. Miller, P. Gupitill, M. Curtis, S. McArdle, and P. Elliot (2000), Active parasitic folds on the Elysian Park anticline: Implications for seismic hazard in central Los Angeles, California, *Geol. Soc. Am. Bull.*, 112(5), 693–707, doi:10.1130/0016-7606(2000)112<693:APFOTE>2.0.CO;2.
- Oskin, M., L. Perg, E. Shelef, M. Strane, E. Gurney, B. Singer, and X. Zhang (2008), Elevated shear zone loading rate during an earthquake cluster in eastern California, *Geology*, 36(6), 507–510, doi:10.1130/G24814A.1.
- Plesch, A., et al. (2007), Community fault model (CFM) for southern California, *Bull. Seismol. Soc. Am.*, 97, 1793–1802, doi:10.1785/0120050211.
- Price, E., and R. Bürgman (2002), Interactions between the Landers and Hector Mine, California, earthquakes from space geodesy, boundary element modeling, and time-dependent friction, *Bull. Seismol. Soc. Am.*, 92(4), 1450–1469, doi:10.1785/0120000924.
- Reid, H. F. (1911), *The elastic-rebound theory of earthquakes*, 444 pp., Univ. of Calif. Press, Berkeley.
- Richards-Dinger, K. B., and P. M. Shearer (2000), Earthquake locations in southern California obtained using source-specific station terms, *J. Geophys. Res.*, 105, 10,939–10,960, doi:10.1029/2000JB900014.
- Rubin, C. M., S. C. Lindvall, and T. K. Rockwell (1998), Evidence for large earthquakes in metropolitan Los Angeles, *Science*, 281, 398–402, doi:10.1126/science.281.5375.398.
- Saucier, F., and E. D. Humphreys (1993), Horizontal crustal deformation in Southern California from joint models of geologic and very long baseline interferometry measurements, in *Contributions of Space Geodesy to Geodynamics—Crustal Dynamics, Geodyn. Ser.*, vol. 23, edited by D. E. Smith and D. L. Turcotte, pp. 139–176, AGU, Washington, D. C.
- Savage, J. C., and R. Burford (1970), Accumulation of tectonic strain in California, *Bull. Seismol. Soc. Am.*, 60, 1877–1896.
- Savage, J. C. (1980), Dislocations in seismology, in *Dislocations in Solids*, vol. 3, edited by F. R. N. Nabarro, pp. 251–339, North-Holland, Amsterdam.
- Savage, J. C. (1983), A dislocation model of strain accumulation and release at a subduction zone, *J. Geophys. Res.*, 88(B6), 4984–4996, doi:10.1029/JB088iB06p04984.
- Savage, J. C. (1990), Equivalent strike-slip earthquake cycles in half-space and lithosphere-asthenosphere Earth models, *J. Geophys. Res.*, 95(B4), 4873–4879, doi:10.1029/JB095iB04p04873.
- Savage, J. C., and R. O. Burford (1973), Geodetic determination of relative plate motion in central California, *J. Geophys. Res.*, 78(5), 832–845, doi:10.1029/JB078i005p00832.
- Savage, J. C., and W. H. Prescott (1978), Asthenosphere readjustment and the earthquake cycle, *J. Geophys. Res.*, 83(B7), 3369–3376, doi:10.1029/JB083iB07p03369.
- Savage, J. C., and R. W. Simpson (1997), Surface strain accumulation and the seismic moment tensor, *Bull. Seismol. Soc. Am.*, 87(5), 1345–1353.
- Schmalzle, G., T. Dixon, R. Malservisi, and R. Govers (2006), Strain accumulation across the Carrizo segment of the San Andreas Fault,

- California: Impact of laterally varying crustal properties, *J. Geophys. Res.*, *111*, B05403, doi:10.1029/2005JB003843.
- Shaw, J., A. Plesch, J. F. Dolan, T. L. Pratt, and P. Fiore (2002), Puente Hills blind-thrust system, Los Angeles California, *Bull. Seismol. Soc. Am.*, *92*(8), 2946–2960, doi:10.1785/0120010291.
- Shen, Z.-K., D. D. Jackson, and B. X. Ge (1996), Crustal deformation across and beyond the Los Angeles basin from geodetic measurements, *J. Geophys. Res.*, *101*(B12), 27,957–27,980, doi:10.1029/96JB02544.
- Simons, M., Y. Fialko, and L. Rivera (2002), Coseismic deformation from the 1999 M_w 7.1 Hector Mine, California, earthquake as inferred from InSAR and GPS observations, *Bull. Seismol. Soc. Am.*, *92*(4), 1390–1402, doi:10.1785/0120000933.
- Stephenson, W. J., T. K. Rockwell, J. K. Odum, K. M. Shedlock, and D. A. Okaya (1995), Seismic reflection and geomorphic characterization of the onshore Palos Verdes Fault Zone, Los Angeles, California, *Bull. Seismol. Soc. Am.*, *85*, 943–950.
- Thatcher, W., G. R. Foulger, B. R. Julian, J. Svarc, E. Quilty, and G. W. Bawden (1999), Present-day deformation across the Basin and Range Province, western United States, *Science*, *283*, 1714–1718, doi:10.1126/science.283.5408.1714.
- Thomas, A. L. (1993), POLY3D: A three-dimensional, polygonal element, displacement discontinuity boundary element computer program with applications to fractures, faults, and cavities in the Earth's crust, Master's thesis, 52 pp. Stanford Univ., Stanford, Calif.
- Tsutsumi, H., R. S. Yeats, and G. J. Huftile (2001), Late Cenozoic tectonics of the northern Los Angeles fault system, California, *Geol. Soc. Am. Bull.*, *113*(4), 454–468, doi:10.1130/0016-7606(2001)113<0454:LCTOTN>2.0.CO;2.
- Tucker, A. Z., and J. F. Dolan (2001), Paleoseismologic evidence for a >8 Ka age of the most recent surface rupture on the eastern Sierra Madre fault, northern Los Angeles Metropolitan region, California, *Bull. Seismol. Soc. Am.*, *91*(2), 232–249, doi:10.1785/0120000093.
- Walls, C., and E. Gath (2001), Tectonic geomorphology and Holocene surface rupture on the Chino fault, paper presented at Southern California Earthquake Center Annual Meeting, Oxnard, Calif.
- Wessel, P., and W. H. F. Smith (1998), New, improved version of the Generic Mapping Tools released, *Eos Trans. AGU*, *79*, 579, doi:10.1029/98EO00426.
- Wright, T. L. (1991), Structural geology and tectonic evolution of the Los Angeles Basin, California, in *Active Margin Basins*, edited by K. T. Biddle, *AAPG Mem.*, *52*, 35–134.
- Yeats, R. (1978), Neogene acceleration of subsidence rates in southern California, *Geology*, *6*, 456–460, doi:10.1130/0091-7613(1978)6<456:NAOSRI>2.0.CO;2.
- Yeats, R. S. (2002), The Chino Fault and its relation to slip on the Elsinore and Whittier faults and blind thrusts in the Puente Hills, final technical report, U.S. Geol. Surv., Reston, Va.
- Yeats, R. S., et al. (1994), Late Cenozoic tectonics of the East Ventura Basin, Transverse Ranges, California, *AAPG Bull.*, *78*(7), 1040–1074.

M. L. Cooke, Geosciences Department, University of Massachusetts Amherst, 611 North Pleasant St., Amherst, MA 01003, USA.

S. T. Marshall, Department of Geology, Appalachian State University, 572 Rivers St., Boone, NC 28608, USA. (marshallst@appstate.edu)

S. E. Owen, Jet Propulsion Laboratory, 4800 Oak Grove Dr., Pasadena, CA 91109, USA.